# Discrete tomography from micro-CT data: application to the mouse trabecular bone structure.

K.J. Batenburg[a,b] and J. Sijbers[c]

[a]Leiden University, The Netherlands;
[b]Centrum voor Wiskunde en Informatica (CWI), Amsterdam, The Netherlands;
[c]Vision Lab, University of Antwerp, Belgium

## ABSTRACT

Discrete Tomography (DT) deals with the reconstruction of an image from its projections when this image is known to have only a small number of gray values. The knowledge of the discrete set of gray values can significantly reduce the number of projections required for a high-quality reconstruction. In this paper, a feasibility study is presented of the application of discrete tomography to micro-CT data from a mouse leg as to study the structural properties of the trabecular bone. The set of gray values is restricted to only three values, for the air background, the soft tissue background, and the trabecular bone structure. Reconstructions of the trabecular bone structure are usually obtained by computing a continuous reconstruction. To extract morphometric information from the reconstruction, the image must be segmented into the different tissue types, which is commonly done by thresholding. In the DT approach such a segmentation step is no longer necessary, as the reconstruction already contains a single gray value for each tissue type. Our results show that by using discrete tomography, a much better reconstruction of the trabecular bone structure can be obtained than by thresholding a continuous reconstruction from the same number of projections.

**Keywords:** Discrete tomography, Micro-CT, Trabecular bone structure

## 1. INTRODUCTION

In the past decades, tomography has become a common tool for medical imaging. Several algorithms are available for the reconstruction of cross-section images from their projections. *Filtered backprojection* is very fast and easy to implement (Chapter 3 of Kak and Slaney[1]). *Algebraic Reconstruction Techniques*, such as ART, SART (Simultaneous Algebraic Reconstruction Techniques) and SIRT (Simultaneous Iterative Reconstruction Techniques) have longer running times but yield better reconstructions in certain cases (Chapter 7 of Kak and Slaney[1]). All these reconstruction methods deal with a *continuous spectrum of gray values*, i.e., the intensities in the reconstruction are real values. In the remainder of this paper, we will use the term *continuous tomography* to denote such methods. Many samples in medical imaging indeed exhibit a wide spectrum of gray values in the reconstructed image. Continuous reconstruction methods require a large number of projections to compute images of sufficient quality, typically more than 100. The number of required projections is directly proportional to the scanning time and, more importantly, the radiation dose.

For certain types of samples, such as the bone sample from a mouse that we study in this paper, each tissue type has its own gray value, which is approximately constant. A continuous reconstruction of such a sample will still contain a large number of different gray values, e.g., due to noise or a lack of projection data. To extract morphometric information from such a reconstruction the image has to be segmented first into the different tissue types, which is usually done by thresholding.[2–4]

Another way of recovering the different tissues from the reconstruction is to use a small, fixed set of gray values during the reconstruction, one for each tissue type. Thereby, the resulting reconstruction does not have to be segmented anymore, as it is already clear which pixel belongs to which tissue. The field of *discrete tomography*

Further author information: (Send correspondence to K.J. Batenburg)
K.J. Batenburg: E-mail: kbatenbu@math.leidenuniv.nl, Telephone: +31 (0)20 5924176
J. Sijbers: WWW: http://webhost.ua.ac.be/visielab/staff/sijbers/, Telephone: +32 (0)3 265.3452

Medical Imaging 2006: Physics of Medical Imaging, edited by Michael J. Flynn, Jiang Hsieh,
Proceedings of SPIE Vol. 6142, 614240, (2006) · 1605-7422/06/$15 · doi: 10.1117/12.652603

deals with tomographic reconstruction problems where the set of gray values is small, discrete and known in advance, see Herman and Kuba[5] for an overview of the field. By incorporating this prior knowledge of the set of gray values directly in the reconstruction algorithm, high quality reconstructions can be obtained from far fewer projections than by continuous tomography. In the extreme case where there are only two gray levels (i.e., black-and-white images), as few as four or five projections are often sufficient to compute an accurate reconstruction, assuming low noise levels.

In this paper, we focus on one particular application which is the reconstruction of the mouse trabecular system. The thickness of trabecular bone is an important architectural parameter of bone strength. Bone growth retardation or age related changes in bone such as osteoporosis, for example, are well known causes of trabecular thinning. While a significant part of the bone's strength % relates to bone density alone, the microstructure of trabecular bone also plays a very important role.[6,7] Many architectural parameters have been measured in cancellous bone and have been tested on their ability to predict fracture risk independent of bone mass.

In order to study the microstructure of the trabecular bone, high quality and high resolution micro-CT images are required. However, the dose needed to obtain such images is many times higher than in clinical CT scanners. The high amount of radiation may have serious consequences for the animal since it might affect bone metabolism. The only option seems to be to scan at lower resolutions, or to limit the dose, which would result in poor image quality. However, as will be shown in this paper, discrete tomography may help to reduce the number of projections (i.e., dose) if the image can be regarded as consisting only of a small number of gray values.

An important step prior to bone structure analysis is the segmentation of the raw, reconstructed gray value images into binary images that only represent bone and non-bone. In other words, for each voxel in the data set, a decision needs to be made whether a voxel is bone or not. This issue becomes even more important when the quality or the resolution of the images is limited as with in-vivo microCT. Simple segmentation methods using a single global threshold value are far from optimal in this case.

But why would one head for high-quality continuous CT reconstructions if, for example by thresholding, most of the information is discarded afterwards? If the goal is, say, to study the morphology of the bone, a high detail reconstruction of the surrounding tissue, or even high gray value resolution of the bone itself, may be of no importance at all. Indeed, to study bone morphology, it might be much more efficient to extract the bone data directly at the reconstruction level. This is where discrete tomography comes into play. By a priori classifying the different structures of the object to be imaged into distinct groups, a high quality reconstruction can be generated from only a small number of projections that resembles the result of a two-stage process consisting of a classical reconstruction with a large number of projections followed by a segmentation procedure.

In this paper, the feasibility of discrete tomography will be demonstrated. In section 2, the principle of discrete tomography will be outlined. In section 3 will focus on a specific application which is the reconstruction of the trabecular bone of the mouse tibia. The results are discussed in section 4 and conclusions are drawn in section 5.

## 2. DISCRETE TOMOGRAPHY

The term *discrete tomography* was first introduced by Larry Shepp in 1994. Advances in electron microscopy gave rise to new types of tomographic reconstruction problems, where the set of possible pixel values of the reconstructed image is very small and known in advance. Originally, the main interest was in reconstructing 3D crystal lattice structures.[8,9] This is a very specific tomography problem, which makes it difficult to extend the obtained results to other tomography settings. Over the past 10 years, focus has moved gradually towards more general tomography settings, including those relevant for medical imaging (see e.g.,[10]).

So far, most results have been obtained for images that contain only two gray levels. For such images, it is usually much easier than for continuous tomography to incorporate additional prior knowledge, such as convexity of the object,[11] local smoothness[12] of the object, Gibbs priors,[13] etc. By using the hard constraint on the set of possible pixel values and combining it with other prior knowledge, it has been shown that for certain types of images, an accurate reconstruction can be computed from very few projections. The type of algorithms that is

used in discrete tomography is very different from continuous tomography. Instead of techniques from analysis (Fourier transforms) and linear algebra, discrete tomography mainly draws from combinatorics and combinatorial optimization, often in combination with techniques from continuous tomography.

Figure 1 shows a phantom image and two reconstructions from five equally spaced projections. The reconstruction in Figure 1b was computed by a discrete tomography algorithm, using the fact that the image is binary as prior knowledge, in combination with a local smoothness prior.[12] The second and third reconstruction, in Figure 1c and e, were obtained by using the filtered backprojection algorithm using 5 and 18 projections, respectively. Finally, Figure 1d and f show the thresholded results of the filtered backprojection reconstructions.

For most biomedical samples, two gray levels are generally not sufficient to represent the different tissues. Few algorithms have been proposed in the literature that deal with more than two gray levels.[13] The discrete tomography results from Section 4 have been obtained with a newly developed algorithm, which will be described in detail in a future publication. The DT algorithm uses iterative algebraic methods and is related to the SIRT (see Chapter 7 of Kak and Slaney[1]). It incorporates a preference for locally homogeneous regions, i.e., regions containing only a single tissue type.

When dealing with several gray levels, the constraint on the set of possible pixel values is not as strong as for the binary case, so more projections are required to obtain an accurate reconstruction. As the number of gray levels increases, the advantage of using discrete gray levels gradually vanishes. To the authors' view, the discrete tomography approach remains interesting if the number of gray levels is below 10 and if no pair of gray levels occurs which are very similar. Even if the same number of projections is required for DT as for continuous tomography, DT still offers the considerable advantage of not requiring any further segmentation.

One of the limitations of the DT approach is that the set of gray values for the different tissue types has to be known in advance. If the gray levels are constant among different samples (i.e., among different animals), this will not be a problem. After computing a high quality continuous reconstruction once, the gray level for each tissue type can be obtained from this reconstruction and used for all subsequent experiments. However, if the gray level of a tissue varies among different samples, the method cannot be applied directly. If several samples (or slices) from the same animal need to be examined, DT can still be used after one of the samples has been reconstructed using continuous tomography. It may be possible to extend our approach to deal with unknown but constant gray levels; this will be considered in future research.

Our reconstruction algorithm is based on the SIRT. In the context of SIRT, the tomographic reconstruction problem is considered as a large linear system

$$\boldsymbol{W}\boldsymbol{x} = \boldsymbol{p} \quad , \tag{1}$$

where the matrix $\boldsymbol{W}$ has dimensions $m \times n$, with $m$ the number of measured line projections and $n$ the number of pixels in the reconstruction. The entry $w_{ij}$ represents the length of the intersection between line $i$ and pixel $j$, see Figure 2. The entries of the $n \times 1$ column vector $\boldsymbol{x}$ represent the gray values of the $n$ pixels. The $m \times 1$ column vector $\boldsymbol{p}$ contains the measured line projections.

The SIRT is an iterative approach for solving the system (1). Let $\boldsymbol{x}$ be a previously computed approximate solution of the system (1). The SIRT algorithm iterates over all lines $i = 1, \ldots, m$, computing

$$\Delta x_j^{(i)} = \frac{p_i - \boldsymbol{w}_{i\cdot}\boldsymbol{x}}{\boldsymbol{w}_{i\cdot}\boldsymbol{w}_{i\cdot}^T} w_{ij} \tag{2}$$

where $\boldsymbol{w}_{i\cdot}$ denotes row $i$ of $\boldsymbol{W}$. Effectively this means that the projection of line $i$ in the current image $\boldsymbol{x}$ (which equals $\boldsymbol{w}_{i\cdot}\boldsymbol{x}$) is subtracted from the prescribed projection $p_i$ in that line. The difference is divided among all pixels $j$ on line $i$, weighted by the intersection length $w_{ij}$. For more details, we refer to book of Kak and Slaney.[1]

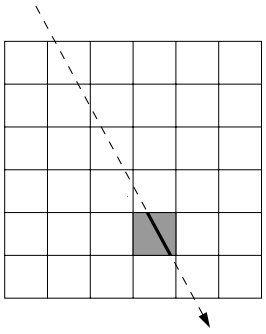

**Figure 2.** The entry $w_{ij}$ denotes the intersection length between ray $i$ and pixel $j$.

After a certain number $T$ of iterations, the continuous reconstruction from the SIRT algorithm is thresholded, assigning each pixel the nearest of the predefined gray levels. The thresholded version of the image is used as the start solution for a new loop of $T$ SIRT iterations.

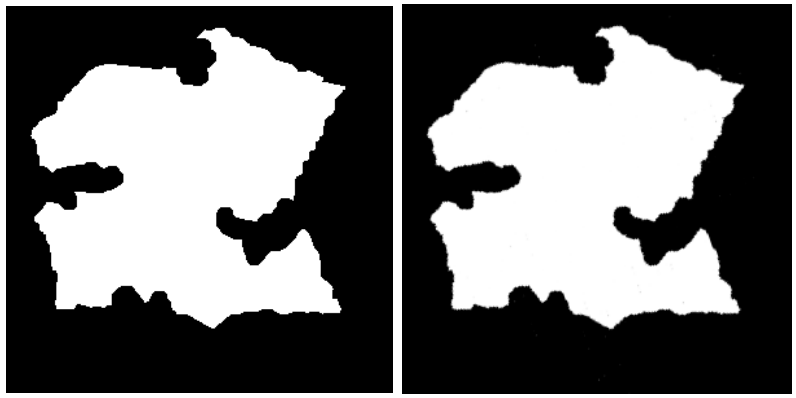

(a) Original image (b) DT (5 proj.)

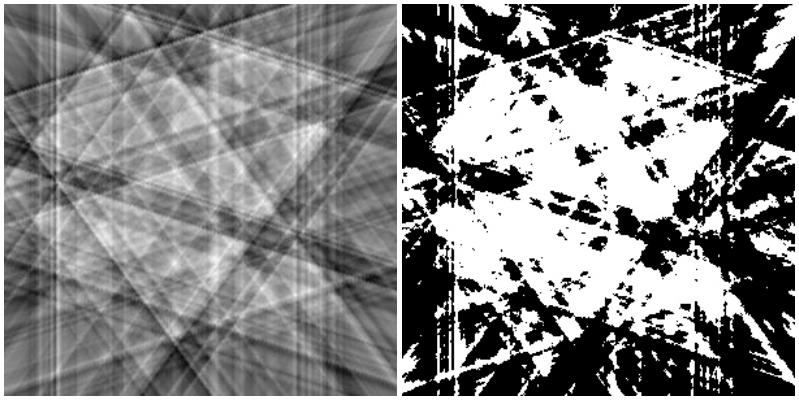

(c) FBP (5 proj.) (d) FBP (5 proj., thresholded)

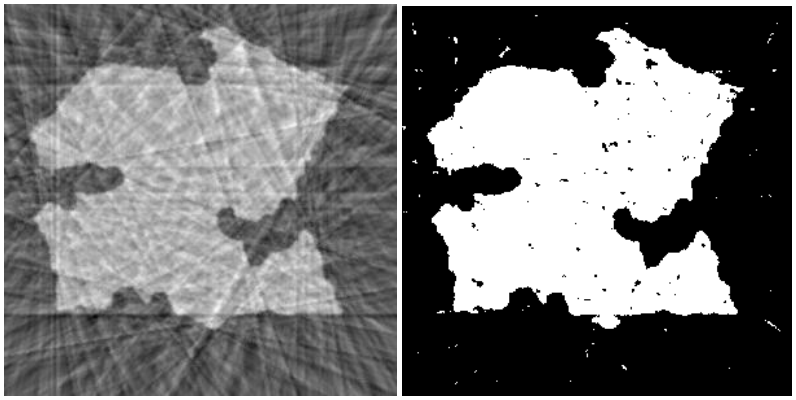

(e) FBP (18 proj.) (f) FBP (18 proj., thresholded)

**Figure 1.** a. Black-and-white phantom image. b. Discrete tomography (DT); reconstruction from 5 projections (0, 36, 72, 108 and 144 degrees); c. Reconstruction from 5 projections using filtered backprojection (FBP); d. Reconstruction using 18 projections using FBP; e. Thresholded result of d.

Errors in the assigned gray levels usually occur at the border between two regions that have different gray levels. Pixels inside a region that has a single gray value are unlikely to be wrong. These pixels are *fixed* for the next set of $T$ SIRT iterations, which means that their value cannot change. If the fixed values are indeed correct, the quality of the remaining part of the reconstruction increases. If a certain fixed pixel $i$ was assigned the wrong gray level, it is likely that different gray levels will show up near pixel $i$ in the new SIRT reconstruction, to

compensate for the wrong value. Therefore, pixel $i$ will no longer be fixed in the next thresholded solution.

## 3. EXPERIMENTS

In this section, we describe all the steps that were followed from acquiring the projection data to computing the reconstructions. The results of this procedure are described in Section 4.

### 3.1. Data acquisition

Data from a mouse proximal tibia were acquired using a micro-CT high resolution SkyScan 1076 in vivo scanner. The mouse was positioned in an aluminum bed with a 40 mm internal diameter.
In order to minimize X-ray absorption of the mouse container, a sample holder of expanded polystyrene was used (see Fig. 3). Due to the negligible absorption of the holder, increase of the noise after reconstruction is prevented.
During acquisition, a cone-beam scanning geometry was employed. The number of projections taken was 200 (the angle step was 0.9 degrees).

**Figure 3.** Proximal tibia scanning using a SkyScan 1076 in vivo scanner (www.skyscan.be).

### 3.2. Data processing

The current algorithm for discrete tomography was developed for parallel beam data (generalization to cone-beam data is feasible, but not yet implemented). Therefore, the optical axis projection data were selected, which were acquired with a fan-beam geometry, and converted to parallel beam data.

Figure 4a shows the parallel beam sinogram that resulted from the rebinning step. It is clear from the sinogram that the object of interest is much smaller than the field of view of the scanner. To speed up the reconstruction algorithm, we only use the part of the sinogram that belongs to the support of the object, i.e., for which the intensity in the sinogram is different from the background intensity.

However, simply discarding the background is not possible, as the background intensity is nonzero. To obtain a background intensity of zero, the sinogram is first inverted, after which the intensity of the background is subtracted uniformly from the image. The resulting sinogram is shown in Figure 4b. Note that the same linear operator is applied to each pixel of the sinogram. It is easy to see that the result of this operation on the reconstructed image is also that a linear operator is applied to each pixel in the reconstruction. Therefore, the actual intensity values in the reconstruction change, but the morphology of the image remains the same. The direct reconstruction from the original sinogram can be obtained from our reconstruction by applying the inverse of this pixel-wise linear operator.

Figure 5 shows the filtered backprojection reconstructions of both sinograms using all 200 projections. Using the sinogram from Figure 4b, we can restrict the reconstruction to a smaller square that contains the bone slice, as the reconstruction should be zero outside this area. Note that the filtered backprojection algorithm does not result in a perfectly zero background.

All reconstructions in Section 4 were computed from the processed sinogram of Figure 4b, using the SIRT algorithm. The reason for using the SIRT algorithm is that it allows for a good comparison with the DT approach, as the DT algorithm is also based on the SIRT. The SIRT reconstructions appear to be of similar quality as the filtered backprojection reconstruction in Figure 5b. All images of continuous reconstructions in Section 4 are actually inverted images of the real reconstructions, to maintain the same gray level ordering between background, sort tissue and bone as in Figure 5a. Figure 9a in Section 4 shows the (inverted) cropped reconstruction in more detail. From this reconstruction, the gray levels of the two different tissue types were determined. The gray

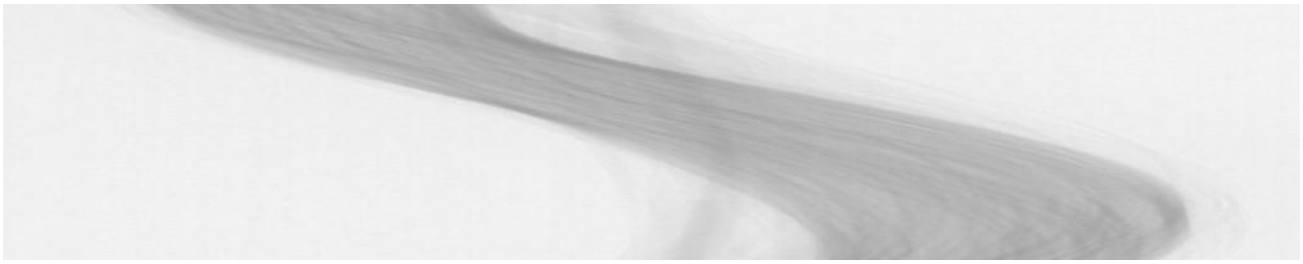

(a) Original sinogram

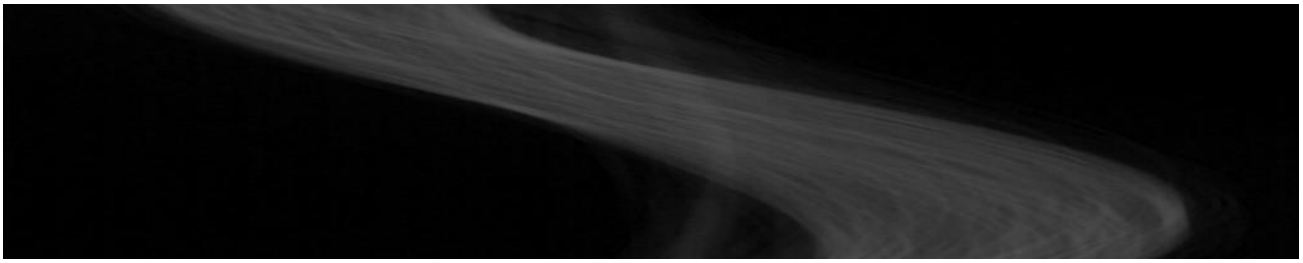

(b) Processed sinogram

**Figure 4.** a. (top): original sinogram, obtained from the SkyScan 1076. b. (bottom): Processed sinogram; the original sinogram was first inverted and then the average intensity of the background was subtracted.

level of the background is obviously zero. The gray levels of the two tissue types are not truly constant, only approximately. For both tissue types, 12 pixels were manually selected in the reconstruction. Table 3.2 shows the average and variance of the gray value in these sets. The input for the discrete tomography algorithm consists of the sinogram of Figure 4b and the list of gray values. The algorithm computes a reconstruction that consists of only those gray values.

| tissue type | average ($\mu$) | standard deviation ($\sigma$) |
|---|---|---|
| background | 0.004 | 0.010 |
| soft tissue | 0.078 | 0.019 |
| trabecular bone | 0.335 | 0.036 |

**Table 1.** Gray values for the background and the two tissue types, determined by manually selecting 15 points of each type in a continuous reconstruction from 200 projections.

## 4. RESULTS AND DISCUSSION

From the fan-beam slice of the cone-beam data set, a number of reconstructions were generated. Figures 6-9 show reconstructions using 25, 40, 67, and 200 projections, respectively. For each image, subfigure (a) denotes a continuous SIRT reconstruction. Subfigures (b) and (c) represent the (globally) thresholded versions of subfigure (a). For both subfigures, two threshold values were selected. The first threshold ($T_1$) is used to separate the soft tissue from the background; the second one, $T_2$ to separate the bone from the soft tissue. For images (b) and (c), $T_1$ was manually selected and fixed for both images. Threshold $T_2$ on the other hand is different in (b) en (c). In (b), $T_2$ is manually chosen as to segment the outer layers of the bone as good as possible. In (c), $T_2$ is manually set as to segment the interior of the bone, this is the trabecular bone structure, as well as possible.

Subfigures (d) and (e) represent reconstructions from discrete tomography based on the same number of projections as used in (a)-(c). In subfigure (d), three discrete gray values were used for the reconstruction process, according to the three gray levels in Table 3.2. In subfigure (e) an additional gray value of 0.045 was

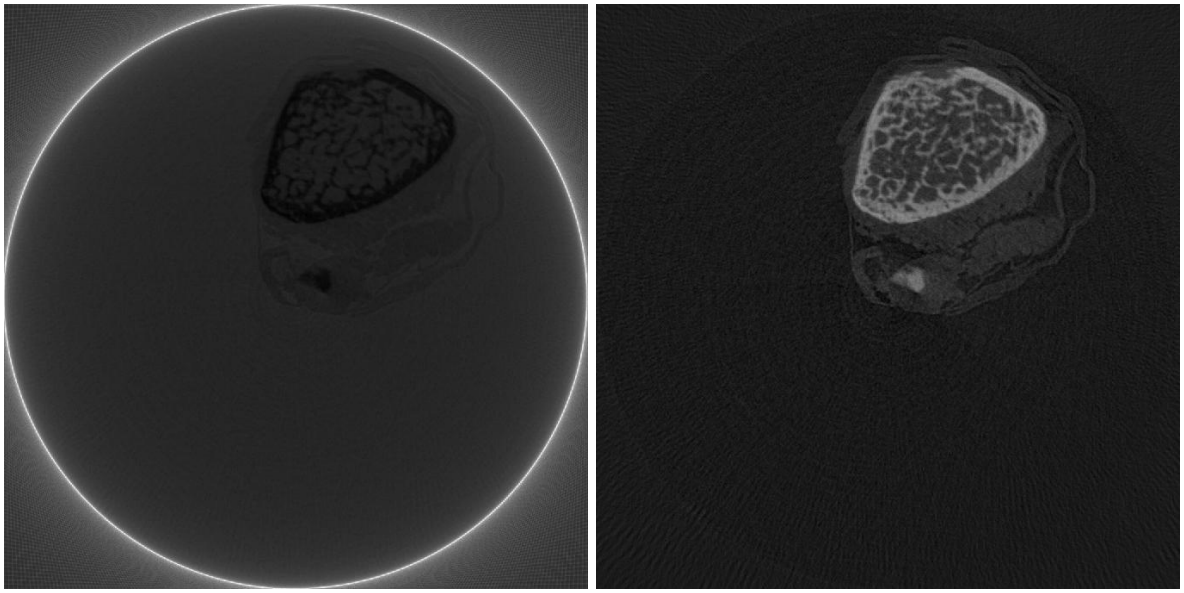

(a) FBP recon. from Fig. 4(a) (b) FBP recon. from Fig. 4(b)

**Figure 5.** a. (top) Filtered backprojection (FBP) reconstruction of the sinogram in Figure 4a using 200 projections. b. (bottom) FBP reconstruction of Figure 4b using 200 projections.

used. After applying the DT algorithm, all pixels in the reconstruction having a gray value of either 0.045 or 0.078 were merged to a single gray value as to represent the soft tissue. The reason for using an additional gray value for the soft tissue is that it appears to give better separation between the soft tissue and the background.

In Figure 6, the results are shown for 25 projections. From subfigures 6(b) and 6(c), it is clear that if as few as 25 projections are used, no global threshold can be found which yields a satisfying segmentation result from the continuous reconstruction in 6(a). On the other hand, the results from discrete tomography are surprisingly close to what would be the correct segmentation result by visual inspection of subfigure 9(a), which shows the continuous reconstruction using the full number of 200 projections. We recall that no threshold has to be selected to attain this result.

From Figure 7 to Figure 9, the number of projections used for the continuous and discrete reconstruction increases from 40 over 67 to 200. Although the segmented results from the continuous reconstructions using more and more projections gradually improve, they are still unsatisfying compared to what can be obtained from discrete tomography. Finally, if the number of projections is 200, the results from continuous and discrete tomography are quite similar.

## 5. CONCLUSION

In this paper, a feasibility study was presented of the application of discrete tomography to micro-CT data from a mouse leg as to study the structural properties of the trabecular bone. The results show clearly that the DT approach yields superior results compared to thresholding of a continuous reconstruction. To obtain good reconstruction results, the DT approach requires far fewer projections. DT already yields good reconstruction quality of the trabecular bone when using as few as 67, or even 40 projections. Using few projections is an important goal, as it limits the radiation dose, which is currently a limiting factor.

It is possible that more sophisticated segmentation algorithms than thresholding can also outperform thresholding. However, it is usually difficult to derive an objective measure of the quality of the segmentation, as the "correct" segmentation is not known. The DT approach yields an objective criterion for the segmentation, based on the measured projection data.

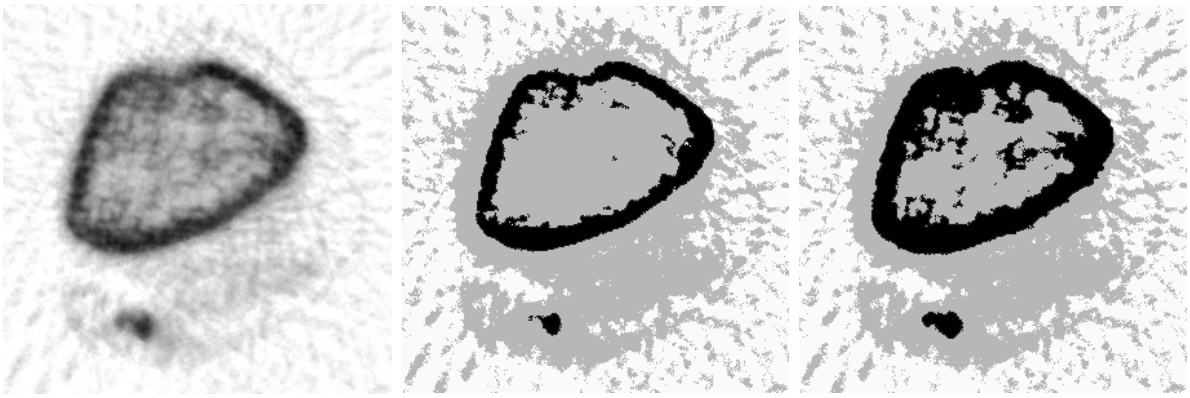

(a) SIRT (b) Low threshold (c) High threshold

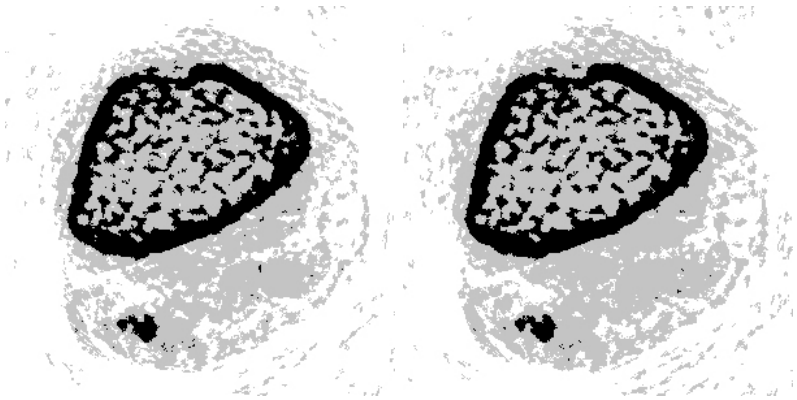

(d) DT (3) (e) DT(4)

**Figure 6.** Reconstructions based on 25 projections

## ACKNOWLEDGMENTS

The research of Joost Batenburg is supported by NWO, The Netherlands. J. Sijbers is a postdoctoral fellow of the F.W.O. (Fund for Scientific Research - Flanders, Belgium). Finally, the authors like to thank Dr. E. Van de Casteele from SkyScan (www.skyscan.be) for providing them with high resolution micro-CT data sets.

## REFERENCES

1. A. C. Kak and M. Slaney, *Principles of Computerized Tomographic Imaging*, SIAM, 2001.
2. M. A. Haidekker, H. Y. Stevens, and J. A. Frangos, "Computerized methods for X-ray-based small bone densitometry," *Computer Methods and Programs in Biomedicine* **73**, pp. 35–42, 2004.
3. D. Last, F. Peyrin, and G. Guillot, "Accuracy of 3D MR microscopy for trabecular bone assessment: a comparative study on calcaneus samples using 3D synchrotron radiation microtomography," *MAGMA Magnetic Resonance Materials in Physics, Biology and Medicine* **18**(1), pp. 26 – 34, 2005.
4. S. Prohaska, H.-C. Hege, M. Giehl, and W. Gowin, "Visual analysis of trabecular bone structure," *J. Grav. Physiol.* **9**(1), pp. 171–172, 2002.
5. G. T. Herman and A. Kuba, eds., *Discrete Tomography: Foundations, Algorithms and Applications*, Birkhäuser, Boston, 1999.
6. J. Sierpowska, M. A. Hakulinen, J. Toyras, J. S. Day, H. Weinans, J. S. Jurvelin, and R. Lappalainen, "Prediction of mechanical properties of human trabecular bone by electrical measurements," *Physiological Measurements* **26**, pp. S119–S131, 2005.

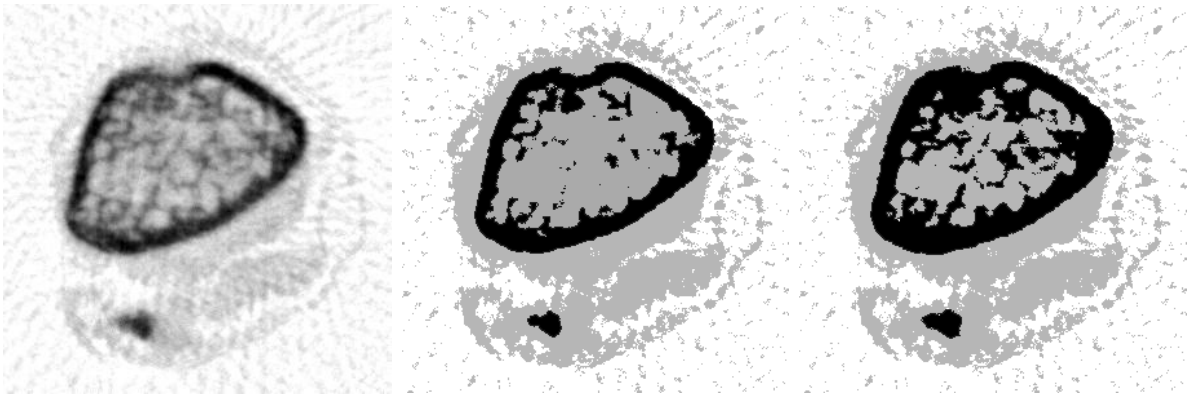

(a) SIRT (b) Low threshold (c) High threshold

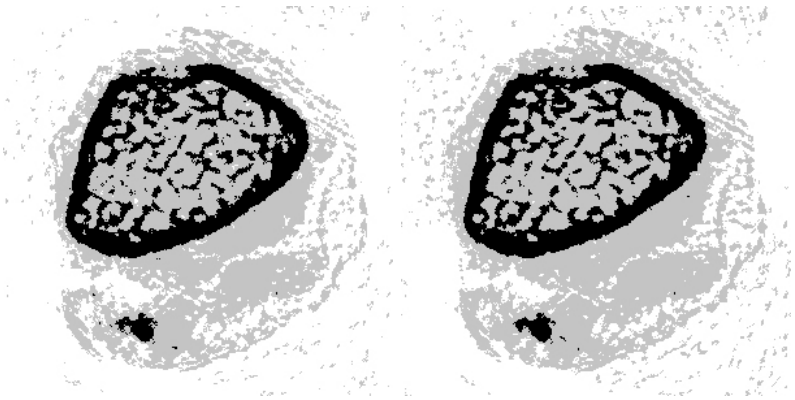

(d) DT(3) (e) DT(4)

**Figure 7.** Reconstructions based on 40 projections


7. T. E. Ciarelli, D. P. Fyhrie, M. B. Schaffler, and S. A. Goldstein, "Variations in three-dimensional cancellous bone architecture of the proximal femur in female hip fractures and in controls," *Journal of Bone Mineral Research* **15**(1), pp. 32–40, 2000.
8. C. Kisielowski, P. Schwander, F. Baumann, M. Seibt, Y. Kim, and A. Ourmazd, "An approach to quantitative high-resolution transmission electron microscopy of crystalline materials," *Ultramicroscopy* **58**, pp. 131–155, 1995.
9. J. R. Jinschek, H. A. Calderon, K. J. Batenburg, V. Radmilovic, and C. Kisielowski, "Discrete Tomography of Ga and InGa Particles From HREM Image Simulation and Exit Wave Reconstruction," *MRS Proceedings* **839**, pp. 4.5.1–4.5.6, 2004.
10. S. Weber, T. Schüle, C. Schnörr, and J. Hornegger, *Bildverarbeitung für die Medizin*, ch. A Linear Programming Approach to Limited Angle 3D Reconstruction from DSA Projections, pp. 41–45. Springer Verlag, March 2003.
11. S. Brunetti, A. D. Lungo, F. D. Ristoro, A. Kuba, and M. Nivat, "Reconstruction of 4- and 8-connected convex discrete sets from row and column projections," *Linear Algebra and its Applications* **339**, pp. 37–57, 2001.
12. K. J. Batenburg, "Reconstructing binary images from discrete X-rays," Tech. Rep. PNA-E0418, CWI, 2004. (Submitted for publication).
13. H. Y. Liao and G. T. Herman, "A coordinate ascent approach to tomographic reconstruction of label images from a few projections," *Discrete Applied Math.* **151**, pp. 181–197, 2005.

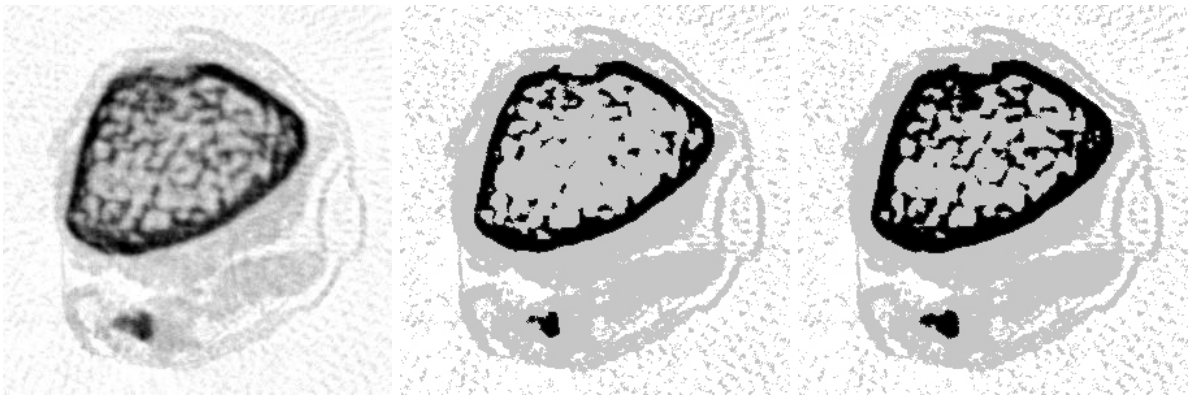

(a) SIRT (b) Low threshold (c) High threshold

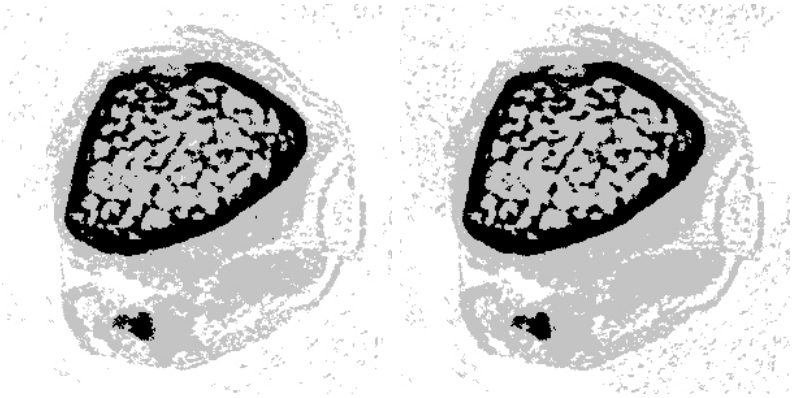

(d) DT(3) (e) DT(4)

**Figure 8.** Reconstructions based on 67 projections

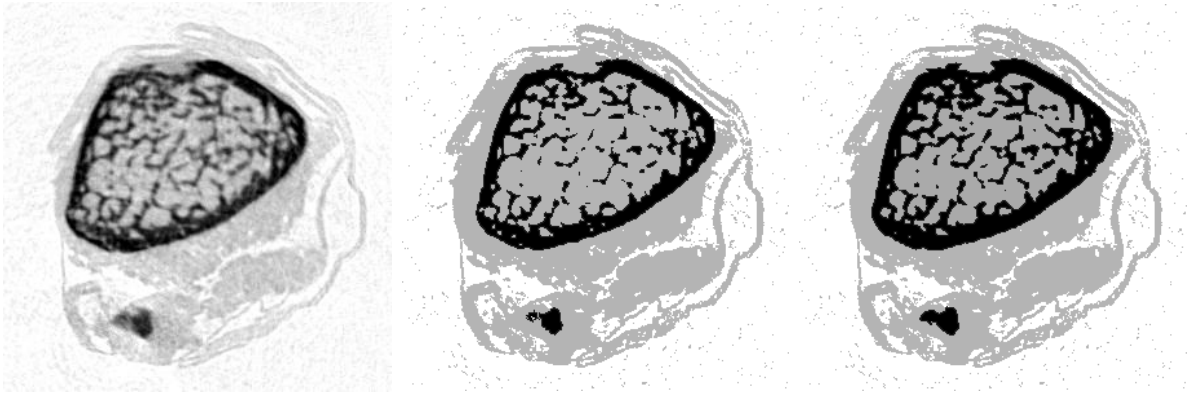

(a) SIRT (b) Low threshold (c) High threshold

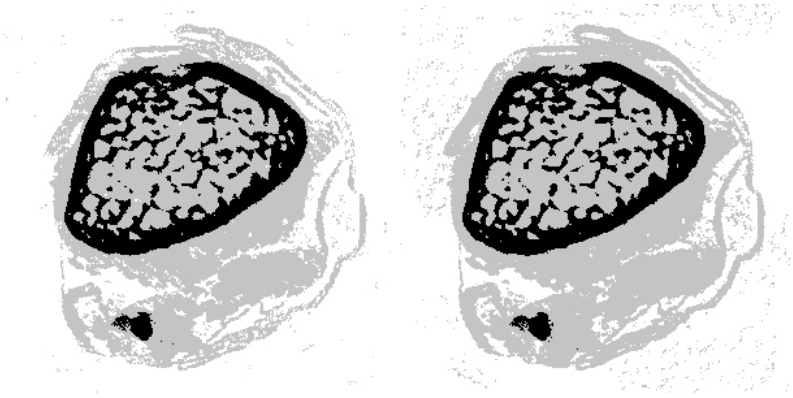

(d) DT(3) (e) DT(4)

**Figure 9.** Reconstructions based on 200 projections